RESEARCH ARTICLE

Experimental study of the remediation of acid mine drainage by Maifan stones combined with SRB

Xuying Guo[1,2]*, **Zhiyong Hu**[1], **Saiou Fu**[3], **Yanrong Dong**[3], **Guoliang Jiang**[3], **Ying Li**[4]

1 College of Mining, Liaoning Technical University, Fuxin, China, **2** College of Science, Liaoning Technical University, Fuxin, China, **3** College of Civil Engineering, Liaoning Technical University, Fuxin, China, **4** Anshan Anqin Group, Anshan, China

* guoxuying@lntu.edu.cn

Abstract

The problems of acid mine drainage (AMD) in coal mine acidic wastewaters arise from a range of sources, including severe pollution with heavy metals and SO_4^{2-} and difficulties during treatment. Based on the ability of Maifan stone to adsorb heavy metals and the dissimilatory reduction of SO_4^{2-} by sulfate-reducing bacteria (SRB), Maifan stone-sulfate-reducing bacterium-immobilized particles were prepared via immobilization techniques using Shandong Maifan stone as the experimental material. The effects of Maifan stones containing SRB on mitigating AMD were investigated by constructing Dynamic Column 1 with Maifan stone-sulfate-reducing bacterium-immobilized particles and by constructing Dynamic Column 2 with SRB mixed with Maifan stones. By the use of adsorption isotherms, adsorption kinetics, a reduction kinetics model and X-ray diffraction (XRD) and scanning electron microscopy (SEM) studies, the mechanism by which Maifan stone-sulfate-reducing bacterium-immobilized particles mitigate AMD was revealed. The results showed that the total effect of Maifan stone-sulfate-reducing bacterium-immobilized particles on AMD was better than that of biological Maifan stone carriers. The highest rates for the removal of Fe^{2+}, Mn^{2+}, and SO_4^{2-} in AMD were 90.51%, 85.75% and 93.61%, respectively, and the pH value of the wastewater increased from 4.08 to 7.64. The isotherms for the adsorption of Fe^{2+} and Mn^{2+} on Maifan stone-sulfate-reducing bacterium-immobilized particles conformed to the output of the Langmuir model. The adsorption kinetics were in accordance with Lagergren first-order kinetics, and the kinetics for the reduction of SO_4^{2-} conformed to those of a first-order reaction model.

1. Introduction

Acid mine drainage (AMD) is polluted water produced by coal mining [1]. Derived from a wide range of sources, AMD exhibits complex water quality, low pH [2], large concentrations of SO_4^{2-} and high concentrations of iron, manganese, copper, zinc and other heavy metals [3]. Direct discharge of AMD substantially pollutes water and soil resources, destroys the

ecological environment, and threatens human health [4]. Currently, the methods commonly used for AMD treatment include the neutralization method [5], constructed wetland method [6,7], adsorption method [8] and microbial method. The adsorption method usually takes advantage of the characteristics of porosity and a large specific surface area of adsorbent to adsorb specific substances in solution to achieve purification [9]. E Wulandari et al. employed natural zeolite and synthetic zeolite to treat AMD, and the removal rates of Cu^{2+} reached 98.16% and 93.98%, respectively [10]. Zheng et al. used iron slag (FS) and carbon steel slag (CSS) from steel mills as adsorbents to remove sulfate from AMD; the results showed that the adsorption capacities of FS and CSS were 225.07 mg.g^{-1} and 320.57 mg.g^{-1}, respectively [11]. The adsorption method has the advantages of simple operation, low cost and availability, but if the adsorption of heavy metal ions is not properly treated, secondary pollution is likely [12]. The microbial method mainly uses SRB to treat AMD [13,14], which can not only remove SO_4^{2-} but also produce alkalinity to improve the pH of waste, which has the advantages of easy access and low treatment cost. Xiao Ye applied sulfate-reducing bacteria (SRB) to remove SO_4^{2-} from acid mine wastewater and achieved a maximum removal rate of 80% [15]. Jennyfer used SRB to remove heavy metals such as As and Fe in AMD; the results showed that the removal rates of As and Fe were 73% and 78%, respectively, [16]. However, SRB had limited tolerance to high metal concentrations and low pH, and high acidity and high concentrations of heavy metal ions inhibit biological activity and harm biological organisms [17].

Microbial immobilization technology is a method that immobilizes microorganisms in a limited space by physical or chemical means to render them highly dense and maintain certain activity [18]. Microbial immobilization, polyvinyl alcohol (PVA), sodium alginate (SA), and other functional groups and carriers of the cementing material resulted in covalent bonds or van der Waals forces and other forms and main chain structure reinforcement. Microorganisms do not easily erode, ensuring that the high-density bacterial group within the microorganism-immobilized particles has high biological activity [18]. Currently, immobilized carrier materials for PVA and SA have large mechanical strength, good mass transfer performance and biological decomposition resistance and other properties. They also have good permeability, are nontoxic and have high transparency [19]. For microbial growth environments, a bacterial pollution system with adaptability and impact resistance ability is improved, and tolerance to heavy metals and pH is enhanced [20,21]. Hong used immobilized spheres to degrade chlorobenzene at a maximum rate of 78.16% [22]. Similarly, Mingliang Zhang [23] employed new immobilized sulfate-reducing bacterium beads that were prepared to treat AMD and obtained a maximum sulfate removal rate of 88%.

Maifan stone has good adsorption; is capable of bidirectional adjustment of the water pH, dissolution and biological activity; and has other advantages. Wen's study showed that Maifan stone has a certain adsorption effect on Mn^{2+}, Pb^{2+}, Cd^{2+}, Cr^{3+} and other metal ions [24], but the adsorption effect on SO_4^{2-} is poor [25]. Zhang Lehong et al. showed that Maifan stone could dissolve a large number of beneficial trace elements, such as selenium and strontium; in particular, the increase rate of selenium reached 178.30%, and the increase rates of the major elements calcium and potassium were 30.30% and 912.50%, respectively [26]. Microorganisms can use these trace elements as nutritional factors to enhance their metabolic activity. Ma Puxi [27] determined that microorganisms can use trace elements released by Maifan stones as nutritional factors to enhance metabolic activity and the effect of denitrification. Jiang Honglin [28] used Maifan stone to prepare a moving bed biofilm reactor, which was applied in the in situ restoration of polluted rivers. The results showed that the chemical oxygen demand, ammonia nitrogen and total nitrogen removal rates of the moving bed biofilm reactor increased by 4.86%, 8.89% and 9.01%, respectively, after the addition of Maifan stone. Therefore, Maifan stone can be embedded during the preparation process of sulfate-reducing

Table 1. Main compositions of Shan Dong Maifan stone.

Constituent	SiO_2	TiO_2	Al_2O_3	Fe_2O_3	MnO	MgO	CaO	Na_2O	K_2O	P_2O_5
Maifan stone	67.90	0.32	15.75	2.82	0.06	0.66	2.51	5.45	1.59	0.056

bacterium-immobilized particles to enhance the biological activity of SRB and improve the treatment effect of immobilized particles on AMD.

In this study, the adsorption method and microbial method were combined with SRB and Shandong Maifan stones using immobilization technology for combination and AMD treatment. The repair effect of Maifan stones and SRB on AMD was explored by constructing a Maifan stone- and sulfate-reducing bacterium-immobilized particle dynamic column and a Maifan stone-loaded sulfate-reducing bacterium dynamic column. The investigation can solve not only the technical bottleneck that single absorption metal ions of Maifan stone cannot remove sulfate root but also the inhibition of sulfate-reducing bacterial activity by heavy metal ions with low pH and high concentrations to ensure that the absorption of Maifan stone and sulfate-reducing bacterium biological activity are advantages of the process of treating acid coal mine wastewater. Combined with the absorption isotherm, adsorption kinetics, reduction kinetics model and X-ray diffraction (XRD), scanning electron microscopy (SEM) detection revealed the mechanism by which Maifan stone-sulfate-reducing bacterium-immobilized particles repair AMD.

2. Materials and methods

2.1 Experimental materials

Shandong Maifan stone: The main chemical constituents of Maifan stone from Linyi City, Shandong Province, China, are shown in Table 1. The Maifan stone was crushed and screened, and a sample with particle sizes ranging from 0.106–0.15 mm (100–150 mesh) was selected. The samples were washed three times with deionized water to remove impurities and then dried at 105°C.

SRB: Activated sludge from the Xihe River, Fuxin city, Liaoning Province, was selected as the strain screening sample. According to Liu's method [29], the bacteria mixed with SRB as the dominant strain were enriched by modified Postgate B medium for subsequent experiments.

Corncob: In this experiment, corncobs was selected as the carbon source for immobilized particles. Corncob contains a rich mixture of organic components and mineral elements that can serve as nutrients for bacteria; it is a stable and inexpensive carbon source. Corncobs from Fuxin farmland with particle sizes ranging from 0.106–0.15 mm were selected.

AMD: Based on the measured water quality data of mine water in a coal mining area of Fuxin City, Liaoning Province, the pH of simulated acid mine wastewater was set to 4, and the concentrations of SO_4^{2-}, Fe^{2+}, Mn^{2+}, Mg^{2+} and Ca^{2+} were 834.5 mg.L^{-1}, 14 mg.L^{-1}, 6 mg.L^{-1}, 50 mg.L^{-1}, and 50 mg.L^{-1}, respectively.

All the chemicals selected for the experiments were analytical reagent grade.

2.2 Experimental method

2.2.1 Preparation of immobilized particles. Nine percent PVA and 0.5% SA were placed in a beaker and stirred until no bubbles existed. SA (0.5%) was added to the bacterial solution of SRB, which was stirred until sticky and set aside. Maifan stone and corn cobs were added to the gel, and the mixture was extracted by a syringe. The mixture was uniformly dripped into
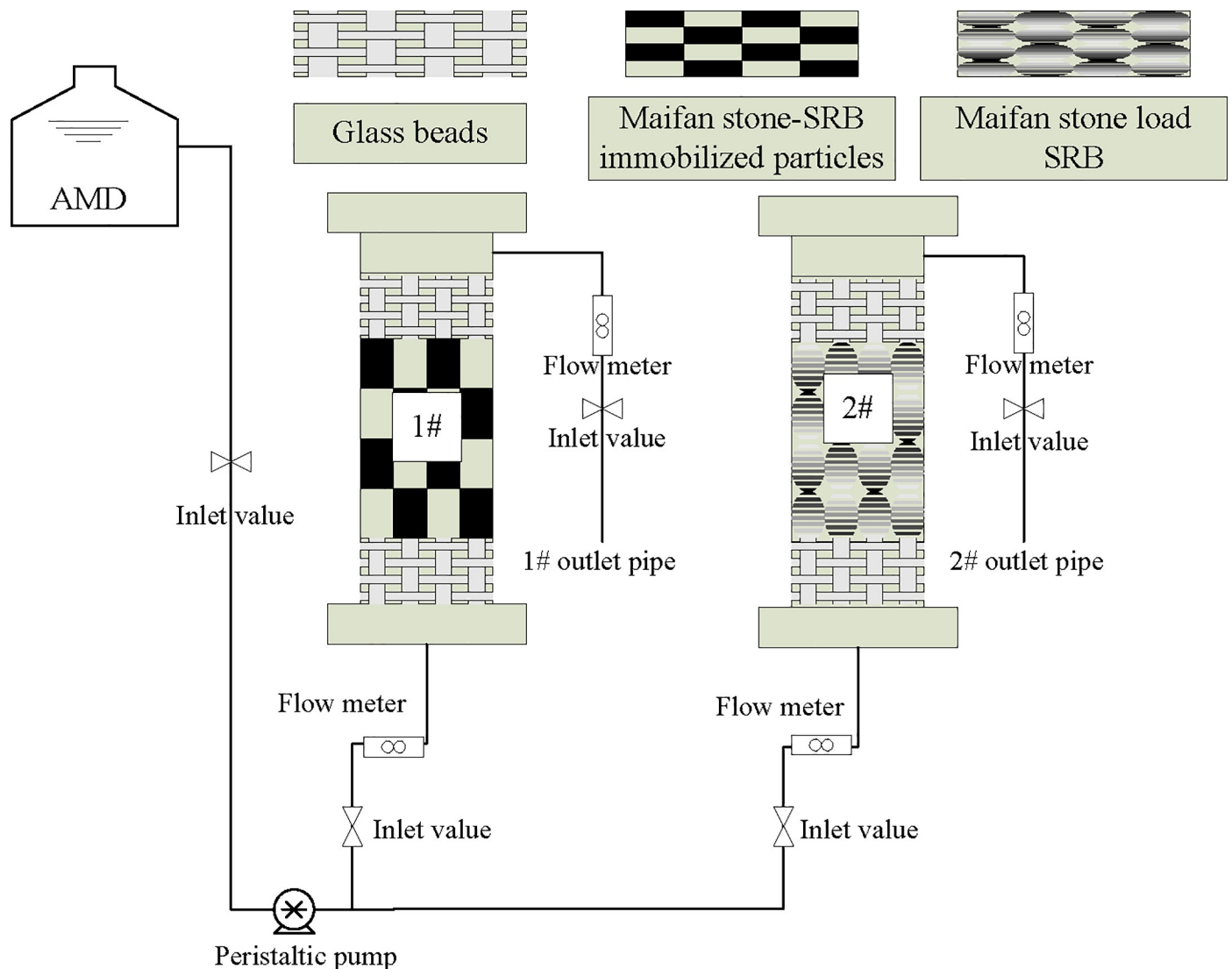
Fig 1. System diagram of the dynamic testing device.

saturated boric acid solution (containing 2% $CaCl_2$, pH 6.0). After addition, the immobilized beads were cross-linked by stirring with a magnetic stirrer for 4 h and then cured.

2.2.2 Construction of the dynamic test device and experimental method. A plexiglass tube with an inner diameter of 6 cm and a height of 50 cm was used to construct the dynamic column of Maifan stone-sulfate-reducing bacterium-immobilized particles and the dynamic column of SRB loaded by Maifan stone, as shown in Fig 1. Column 1 was filled with immobilized particles with a height of 40 cm, and Column 2 was filled with the same amount of Maifan stone, SRB and corn cob. Glass beads were added at the upper and lower ends of the dynamic columns and served as buffer protection layers. AMD was imported into the lower inlet of the dynamic column by a peristaltic pump; the hydraulic load in the dynamic column was controlled at 0.314 $m^3/(m^2/day)$; and the hydraulic retention time was 12.21 h. Samples of water were collected regularly every day. The pH values and residual concentrations of Fe^{2+}, Mn^{2+} and SO_4^{2-} in the effluent were determined. Each group of experiments was repeated 3 times, and the mean value was obtained. The formula for calculation of removal efficiency η is

expressed as follows:

$$\eta = \frac{C_0 - C_t}{C_0} \times 100\% \qquad (1)$$

where C_0 (mg.L^{-1}) is the initial concentration of Fe^{2+}, Mn^{2+} or SO$_4^{2-}$ and C_t (mg.L^{-1}) is the residual concentration of Fe^{2+}, Mn^{2+} or SO$_4^{2-}$ in the effluent of the dynamic column at time t.

2.2.3 Test method for adsorption kinetics of Fe^{2+} and Mn^{2+}. Solutions containing 30 mg.L^{-1} Fe^{2+} and 15 mg.L^{-1} Mn^{2+} were prepared. Next, 100 mL of solution was added to a 250 mL conical flask, and the immobilized particles were added at a ratio of 1:10 (g.mL^{-1}). After shaking for 1, 2, 3, 4, and 5 days at 35°C and 150 r/min, the residual concentrations of Fe^{2+} and Mn^{2+} in the solution were determined, and the adsorption capacity q of Maifan stone-sulfate-reducing bacterium-immobilized particles for Fe^{2+} and Mn^{2+} was calculated. Each group of experiments was repeated 3 times, and the mean value was obtained.

2.2.4 Adsorption isotherms of Fe^{2+} and Mn^{2+}. Fe^{2+} isothermal adsorption test: 100 mL of solutions with different Fe^{2+} concentrations (initial concentrations were 10 mg.L^{-1}, 20 mg.L^{-1}, 30 mg.L^{-1}, 40 mg.L^{-1} and 50 mg.L^{-1}) were added to 250 mL conical flasks, and immobilized particles were added to give solid-liquid ratios of 1:10 (g/mL). After oscillation at 35°C and 150 r/min for 5 days, the concentration of Fe^{2+} remaining in the solution was determined, and the adsorption capacity q of Maifan stone-sulfate-reducing bacterium-immobilized particles for Fe^{2+} was calculated. Each group of experiments was repeated 3 times, and the mean value was obtained.

Isothermal adsorption of Mn^{2+}: Preparation of different concentrations of Mn^{2+} solution (initial concentrations were 5 mg.L^{-1}, 10 mg.L^{-1}, 15 mg.L^{-1}, 20 mg.L^{-1}, 25 mg.L^{-1}); the other conditions were the same as those previously described. The formula for calculation of adsorption q was

$$q = \frac{(C_0 - C_t) \times V}{m} \qquad (2)$$

where C_0 is the initial concentration of ions to be measured (mg.L^{-1}), C_t is the residual concentration after adsorption (mg.L^{-1}), V is the solution volume (L), and m is the mass of immobilized particles (g).

2.2.5 Water quality detection and material characterization methods. Fe^{2+} concentrations were determined by o-phenanthroline spectrophotometry (HJ/T 345–2007), Mn^{2+} content was determined by potassium periodate spectrophotometry (GB 11906–89), SO$_4^{2-}$ content was determined by barium chromate spectrophotometry (HJ/T 342–2007), pH was determined with the glass electrode method (GB 6920–86), and Eh was measured by a Pen redox potentiometer.

SEM (3400 N) was employed to analyze the morphological properties of Shandong Maifan stones, Maifan stone-sulfate-reducing bacterium-immobilized particles, Maifan stone-sulfate-reducing bacterium-immobilized particles after AMD treatment and Maifan stone-loaded SRB after AMD treatment. XRD (D/MAX2400) was used to analyze the mineral compositions of Shandong Maifan stones, Maifan stone-sulfate-reducing bacterium-immobilized particles, Maifan stone-sulfate-reducing bacterium-immobilized particles after AMD treatment, and Maifan stone-loaded SRB after AMD treatment.

3. Results and discussion

3.1 Dynamic test of Maifan stones combined with SRB for mitigation of AMD

The experimental results for the column containing sulfate-reducing bacterium-immobilized particles (Dynamic Column 1) and the column containing Maifan stone loaded with SRB (Dynamic Column 2) in treating AMD are shown in Fig 2.

3.1.1 Removal percentage of Fe^{2+}. Fig 2(a) shows that the percentages of Fe^{2+} in AMD removed by Dynamic Columns 1 and 2 initially increased and then decreased. From 1 to 6 days, the percentages of Fe^{2+} removal by Dynamic Column 1 and Dynamic Column 2 increased from 38.79% and 35.04% to 90.51% and 88.73%, respectively. The removal of Fe^{2+} mainly depends on the adsorption of Maifan stone [30], ion exchange [31] and precipitation. SRB produces S^{2-} [32] due to the reduction [33] of SO$_4^{2-}$, which forms a precipitate with Fe^{2+}. Additionally, the removal of Fe^{2+} was enhanced because the negative charge on the surface of SRB [34] facilitates electrostatic adsorption of Fe$^{2+,}$ and the sulfate-reducing bacterium extracellular polymer also affects biological flocculation of Fe^{2+} [35]. The removal of Fe^{2+} by Dynamic Column 1 stabilized in 7–15 days; and the removal of Fe^{2+} by Dynamic Column 2 continued to evolve. The removal of Fe^{2+} in AMD with Dynamic Column 1 was more effective than that with Dynamic Column 2, which indicated that the technology based on immobilized particles prolonged the biological activity of SRB and improved the removal efficiency of Fe^{2+}.

(a) Removal of Fe^{2+} (%)

(b) Removal of Mn^{2+} (%)

(c) Removal of SO$_4^{2-}$ (%)
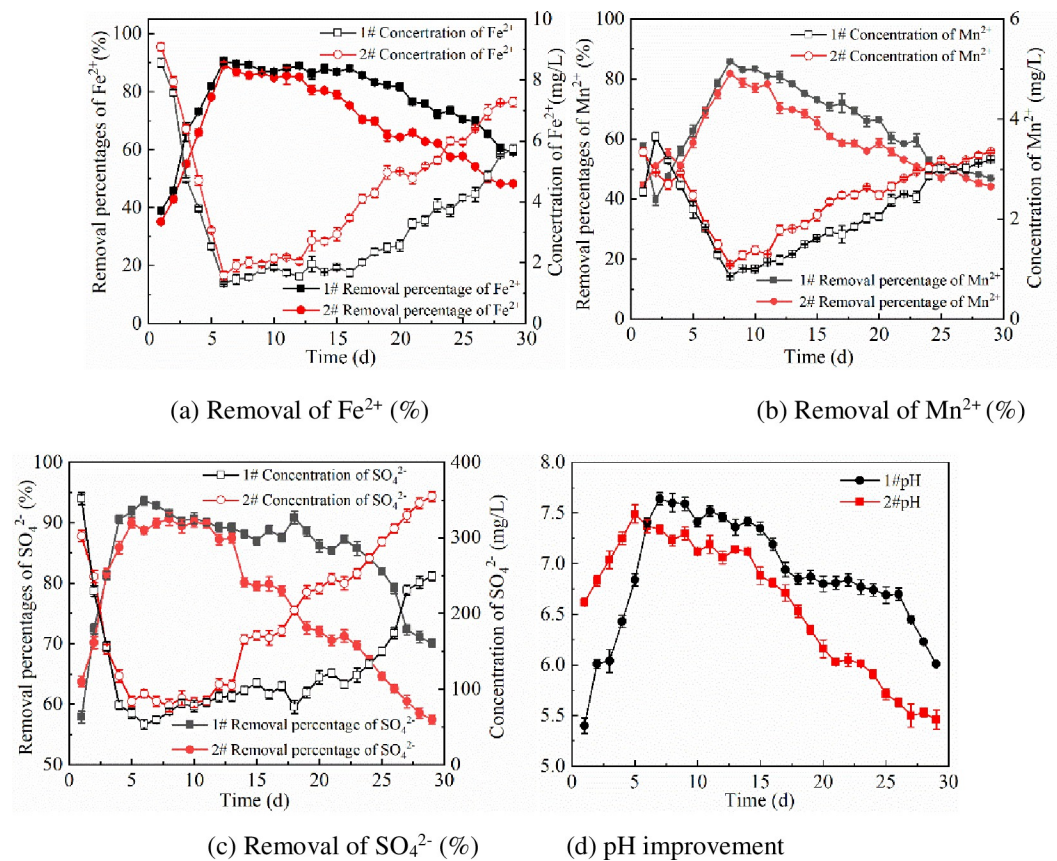
(d) pH improvement

Fig 2. Removal effect of Dynamic Columns 1 and 2 with AMD. (a) Removal of Fe^{2+} (%). (b) Removal of Mn^{2+} (%). (c) Removal of SO$_4^{2-}$ (%). (d) pH improvement.

https://doi.org/10.1371/journal.pone.0261823.g002

During the period 20–30 days, the levels of Fe^{2+} removal by Columns 1 and 2 decreased gradually because the pores of Maifan stones were blocked after substantial periods of adsorption, thus affecting adsorption. The gradual accumulation of heavy metals in wastewater would make the wastewater toxic toward SRB and serve to reduce sulfate-reducing bacterial activity, thereby inhibiting the removal of Fe^{2+}.

3.1.2 Removal percentage of Mn^{2+}. Fig 2(b) shows that the efficiency of Mn^{2+} removal from AMD by Dynamic Columns 1 and 2 initially increased and then decreased. From day 1 to day 8, the removal efficiencies increased from 57.53% and 44.28% to 85.75% and 81.83%, respectively. On the 8th day, the residual Mn^{2+} concentrations were 0.86 mg.L^{-1} and 1.09 mg.L^{-1}, respectively. On the 8th day, the removal efficiency for Mn^{2+} began to decrease. The efficiency of Mn^{2+} removal was lower than that of Fe^{2+} because the mechanisms for adsorption of Fe^{2+} and Mn^{2+} in the system differed [36]. SRB in columns 1 and 2 reduced SO_4^{2-} to S^{2-}, which combined with Mn^{2+} to form MnS precipitates. When Mn^{2+} in the system accumulated to a certain concentration, SRB began to die, thereby affecting the removal of Mn^{2+}. In addition, due to its large solubility constant, MnS easily dissolves in a weakly acidic environment, and Mn^{2+} cannot be completely removed by precipitation. Therefore, the efficiency of Mn^{2+} removal is lower than that of Fe^{2+}.

3.1.3 Removal percentage of SO_4^{2-}. Fig 2(c) shows that the removal of SO_4^{2-} in AMD by Dynamic Columns 1 and 2 initially increased and then decreased, and column 1 was significantly better than column 2. From 1 to 6 days, the SO_4^{2-} removal efficiency of Dynamic Column 1 increased from 57.86% to 93.61%. On days 1–8, the removal efficiency of Dynamic Column 2 increased from 63.74% to 90.62%. Since the corncobs in the system released organic matter with nutrients supporting the growth of SRB, a sufficient carbon source and appropriate COD/SO_4^{2-} enhanced the activity of SRB in the system [37]. This finding is conducive to the dissociation and reduction of SO_4^{2-} and thereby enhances the removal of SO_4^{2-}, which shows an upward trend. On days 7–22, the performance of Dynamic Column 1 tended to stabilize.

On days 9–13, dynamic column 2 tended to stabilize. The efficiency of column 1 during the period of stability was better than that of column 2, which indicated that immobilization technology slowly released organic matter and improved sulfate-reducing bacterium biological activity over the long term. At later stages of the reaction, the removal efficiency of SO_4^{2-} decreased due to a gradual decrease in the amount of organic matter released and the inhibition of sulfate-reducing bacterial activity caused by high concentrations of heavy metal ions resulting from continuous inflow. Comprehensive analysis of SO_4^{2-} removal indicated that the efficiency of column 1 was greater than that of column 2.

3.1.4 pH improvement. Fig 2(d) shows that Dynamic Columns 1 and 2 initially affected increases and then affected decreases in the pH of AMD. Columns 1 and 2 increased the initial pH value from 4.08 to 7.64 and 7.49, respectively. At the early stages, the main factor causing increases in pH values was the ability of Maifan stones to affect bidirectional regulation [38]. From 1 to 5 days, the pH of the AMD treated by Dynamic Column 2 increased more than that of AMD treated in Dynamic Column 1, because direct treatment of wastewater by SRB consumed H^+ [39] and the pH of the wastewater increased significantly. Simultaneously, SRB decomposes the carbon source in the environment to produce HCO_3^- through biological metabolism, which increases the pH value and alkalinity of the solution [39]. After 5 days, the HCO_3^- content increases with a continuous anaerobic reaction of sulfate-reducing bacterium-dominated sulfate reduction [40]. The effluent pH of Dynamic Column 1 continued to rise, stabilized and then decreased slowly; the pH of the effluent treated in Dynamic Column 2 continued to decline. The improvement in pH affected by Dynamic Column 1 was significantly better than that of Dynamic Column 2.

3.1.5 Effect analysis of repairing AMD.   A comprehensive analysis showed that during the use of Dynamic Columns 1 and 2 for the removal of Fe^{2+}, Mn^{2+}, and SO_4^{2-} and an increase in pH, the performance of Column 1 was better than that of Column 2. The highest removal rates of Fe^{2+}, Mn^{2+} and SO_4^{2-} by dynamic column 1 were 90.51%, 85.75% and 93.61%, respectively, and the pH value of wastewater increased from 4.08 to 7.64. Previous studies showed that when Maifan stone is used to treat AMD, the removal rates of SO_4^{2-}, Fe^{2+} and Mn^{2+} in mine acid wastewater are 6.87%, 68.9% and 32.8%, respectively [41]. The average removal rates of SO_4^{2-} and Mn^{2+} by SRB for AMD were 61.63% and 72.35%, respectively [42]. The effect of direct remediation of Fe^{2+}, Mn^{2+} and SO_4^{2-} pollutants in AMD with Dynamic Column 1 and Maifan stone was analyzed. The results confirmed that immobilization technology could improve the adaptability, shock resistance and low pH tolerance of the bacteria in the polluted system to improve the remediation effect.

3.2 Adsorption isotherms and kinetic analysis of immobilized particles

3.2.1 Analysis of adsorption isotherms for Fe^{2+} and Mn^{2+}.   Langmuir and Freundlich adsorption isotherm models were used to analyze the adsorption isotherms of Fe^{2+} and Mn^{2+} on Maifan stone-sulfate-reducing bacterium-immobilized particles. The fitting results are shown in Fig 3.

$$\text{Langmuir adsorption isotherm equation}: \quad \frac{c_e}{q_e} = \frac{1}{q_m k_L} + \frac{c_e}{q_m} \tag{3}$$

where q_e (mg.g^{-1}) is the amount of metal ions adsorbed per unit mass of adsorbent at equilibrium; c_e (mg.L^{-1}) is the equilibrium concentration of solute in the bulk solution; q_m is the saturated adsorption capacity; and K_L is the Langmuir model adsorption constant.

$$\text{Freundlich adsorption isotherm equation}: \quad q_e = k_f c_e^{1/n} \tag{4}$$

where q_e (mg.g^{-1}) is the amount of metal ions adsorbed per unit mass of adsorbent at equilibrium, Ce (mg.L^{-1}) is the equilibrium concentration of solute in the bulk solution, k_L is the Freundlich model adsorption constant, and n is the correlation coefficient of adsorption strength.
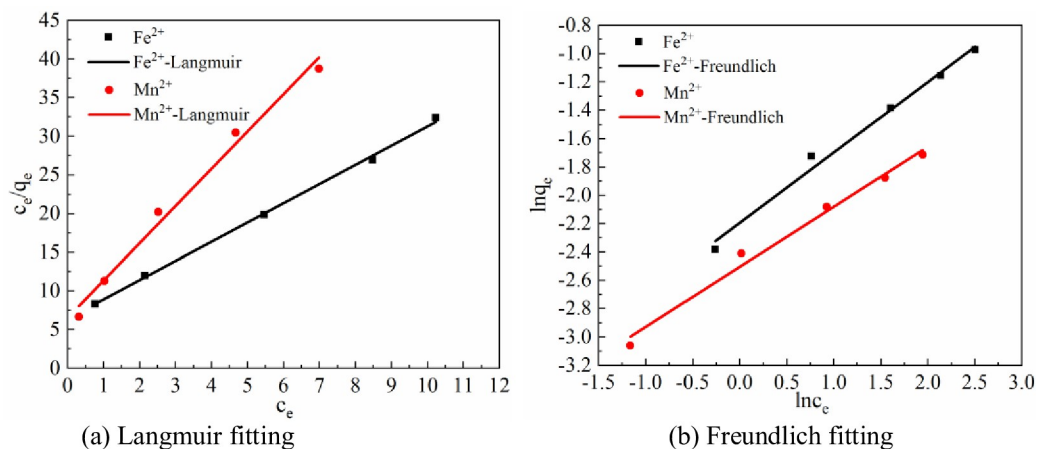

(a) Langmuir fitting   (b) Freundlich fitting

Fig 3. Isotherms for adsorption of Fe^{2+} and Mn^{2+} on immobilized particles. (a) Langmuir fitting. (b) Freundlich fitting.

According to Fig 3, the Langmuir fit to the curve for the removal of Fe^{2+} by Maifan stone-sulfate-reducing bacterium-immobilized particles was $c_e/q_e = 6.43737c_e + 2.48397$, and $R^2 = 0.99754$. The Freundlich fitting curve equation was $\ln q_e = 0.49634 \ln ce - 2.19336$, $R^2 = 0.9859$. The Langmuir fitting curve equation for Mn^{2+} removal by the Maifan stone-sulfate-reducing bacterium-immobilized particles was $c_e/q = 4.8172c_e + 6.54707$, $R^2 = 0.98428$. The Freundlich fitting curve equation was $\ln q_e = 0.42396 \ln c_e - 2.50475$, $R^2 = 0.98332$. A comparison of the correlation coefficients R^2 reveal that those for the Langmuir fits for adsorption of Fe^{2+} and Mn^{2+} by the immobilized particles were higher, so the adsorption of Fe^{2+} and Mn^{2+} in solution by the immobilized particles was more consistent with the Langmuir model. This finding indicated that the adsorption process of Fe^{2+} and Mn^{2+} by particles was dominated by monolayer adsorption. As the adsorption sites were gradually occupied, the adsorption rate gradually decreased until equilibrium was reached.

Comparing the saturated adsorption capacity q_m, the adsorption capacity of Maifan stone-sulfate-reducing bacterium-immobilized particles on Fe^{2+} is stronger. The Freundlich constants of Fe^{2+} and Mn^{2+} are 0.49634 and 0.42396, respectively; both are less than 0.5. This finding shows that the adsorption of Fe^{2+} and Mn^{2+} is relatively easy for Maifan stone-sulfate-reducing bacterium-immobilized particles.

3.2.2 Analysis of adsorption kinetics for Fe^{2+} and Mn^{2+}. The Lagergren first-order dynamic model, Lagergren second-order dynamic model and intraparticle diffusion model were used to analyze the kinetics for the adsorption of Fe^{2+} and Mn^{2+} on Maifan stone-sulfate-reducing bacterium-immobilized particles. The fitting results are shown in Fig 4 and Table 2.

$$\text{First-order model}: \ln(q_e - q_t) = \ln q_e - k_1 t \tag{5}$$

where q_e (mg.g^{-1}) and qt (mg.g^{-1}) are the amounts of adsorbed adsorbate at equilibrium and at time t, respectively, and k1 (min^{-1}) is the rate constant of pseudo-first-order adsorption.

$$\text{Second-order model}: \frac{t}{q_t} = \frac{1}{k_2 q_e^2} + \frac{t}{q_e} \tag{6}$$

where k_2 (mg.(g.min))$^{-1}$ is the equilibrium rate constant of pseudo-second-order adsorption and qe (mg. g^{-1}) and qt (mg.g^{-1}) are the amounts of adsorbed adsorbate at equilibrium and at time t.

$$\text{Intraparticle diffusion model}: q_t = k_p t^{1/2} \tag{7}$$
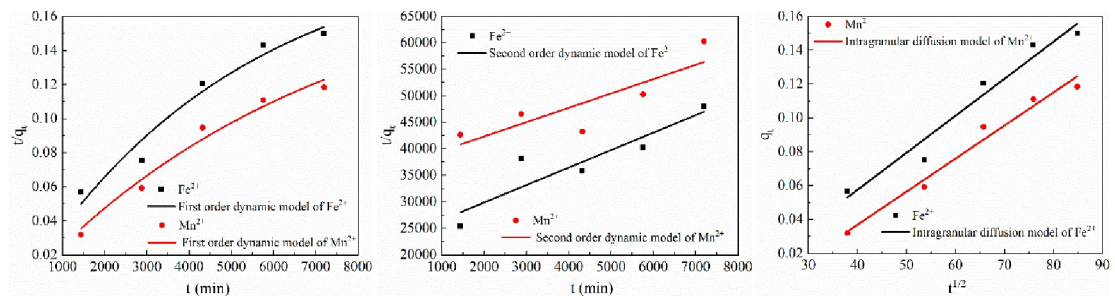
(a) First-order dynamic model   (b) Second-order dynamic model   (c) Intraparticle diffusion model

Fig 4. Results for fitting kinetics for adsorption of Fe^{2+} and Mn^{2+} on immobilized particles. (a) First-order dynamic model. (b) Second-order dynamic model. (c) Intraparticle diffusion model.

Table 2. Kinetic parameters of adsorption of Fe^{2+} and Mn^{2+} by immobilized particles.

kinetic model	parameter	Fe^{2+}	Mn^{2+}
First-order dynamic model	k_1	1.94074×10^{-4}	1.41278×10^{-4}
	q_e	0.20428	0.1924
	R^2	0.94912	0.97054
Second-order dynamic model	k_2	4.66513×10^{-4}	1.44388×10^{-4}
	q_e	0.30337	0.41585
	R^2	0.78206	0.64092
Intraparticle diffusion model	k_p	0.00219	0.00196
	c	-0.03005	-0.0414
	R^2	0.94433	0.9678

where q_t (mg.g^{-1}) is the amount of solute on the surface of the sorbent at time t and k_p (mg.(g. min$^{1/2}$)$^{-1}$) is the intraparticle diffusion rate constant.

Table 2 and Fig 4 show that when the data for Fe^{2+} adsorption by Maifan stone-sulfate-reducing bacterium-immobilized particles were treated with the first-order adsorption kinetics model, second-order adsorption kinetics model and intraparticle diffusion model, the fit of the data yielded correlation coefficients R^2 of 0.94912, 0.78206 and 0.94433, respectively. The first-order kinetic model had a greater correlation coefficient, so the adsorption of Fe^{2+} by Maifan stone-sulfate-reducing bacterium-immobilized particles was more consistent with the first-order kinetic model: $q_t = q_t = 0.20428 \times (1 - e^{-1.94074 \times 10^{-4} t})$, $R^2 = 0.98428$. When Mn^{2+} was adsorbed by Maifan stone-sulfate-reducing bacterium-immobilized particles, the first-order adsorption kinetic model ($R^2 = 0.97054$) exhibited a greater correlation coefficient than the second-order adsorption kinetic model ($R^2 = 0.64092$) and intraparticle diffusion model ($R^2 = 0.9678$). Therefore, the adsorption of Mn^{2+} by Maifan stone-sulfate-reducing bacterium-immobilized particles was also more consistent with the first-order adsorption kinetics model: $q_t = 0.1924 \times (1 - e^{-1.41278 \times 10^{-4} t})$, $R^2 = 0.97054$. The q_e obtained by fitting the equations was greater than the amount of equilibrium adsorption at the experimental node, that is, at t = 5 days, indicating that the adsorption of Fe^{2+} and Mn^{2+} by immobilized particles did not reach the saturation state.

3.2.3 Analysis of reduction kinetics test results of SO_4^{2-}. First-order kinetic and zero-order kinetic models were employed to analyze the reduction of SO_4^{2-} by Maifan stone-sulfate-reducing bacterium-immobilized particles. The fitting results are shown in Fig 5.

Fig 5 shows that the equation for the zero-order dynamic fit to data from the reduction of SO_4^{2-} by immobilized particles was $c_t = 542.828 - 0.06856\, t$, $R^2 = 0.96314$, and the first-order dynamic fitting equation was $\ln c_t = 6.68937 - 3.19398 \times 10^{-4}\, t$, $R^2 = 0.96865$. The correlation coefficient for the first-order kinetics fit was greater than that of the zero-order kinetics fit, indicating that the reduction of SO_4^{2-} by immobilized particles is more consistent with the first-order kinetics model. Furthermore, the electron acceptor was the main factor affecting the reduction of SO_4^{2-} by SRB.

3.3 Mechanistic analysis of AMD mitigation by Maifan stones combined with SRB

3.3.1 XRD analysis. Fig 6 shows the XRD data for Shandong Maifan stones combined with Maifan stone-sulfate-reducing bacterium-immobilized particles and with SRB loaded with Maifan stones, before and after AMD mitigation.
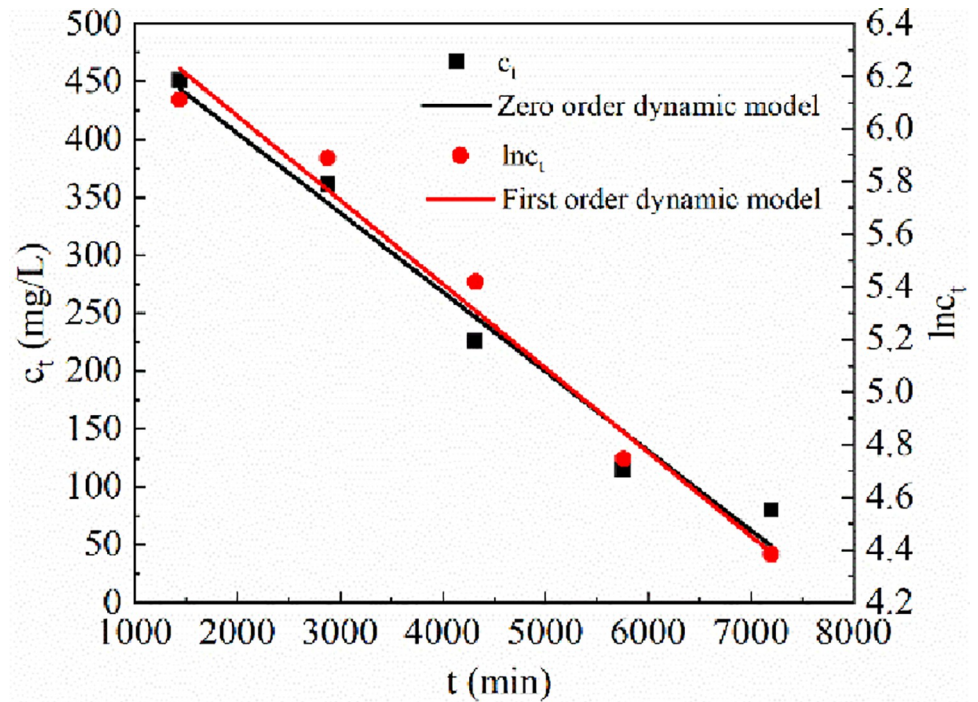
Fig 5. First-order kinetic and zero-order kinetic models of SO_4^{2-}.

Fig 6(a) shows that Maifan stone-sulfate-reducing bacterium immobilized particles exhibit typical peak characteristics of Maifan stones, such as those for quartz and potash feldspar, plagioclase, kaolin, PVA and SA [43]. The immobilized particles of Maifan stone-sulfate-reducing bacterium and Maifan stone showed similar XRD patterns, indicating that the immobilization
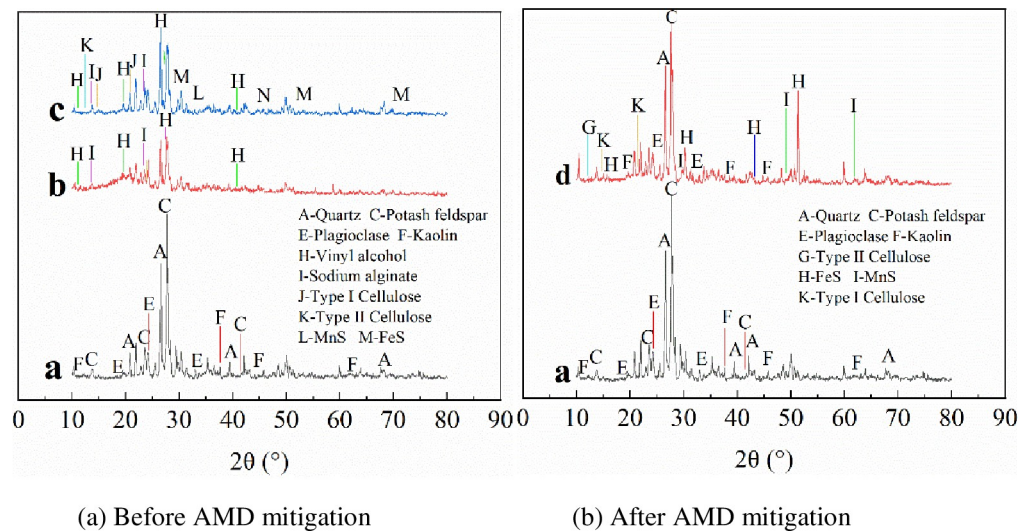

(a) Before AMD mitigation

(b) After AMD mitigation

Fig 6. XRD patterns of Maifan stones combined with SRB before and after AMD repair. (a) Before AMD mitigation. (b) After AMD mitigation. a: Shandong Maifan stone; b: Before treatment of AMD with Maifan stone sulfate-reducing bacterium-immobilized particles; c: After treatment of AMD with Maifan stone sulfate-reducing bacterium-immobilized particles; d: Treatment of AMD by SRB loaded with Maifan stone.

technology had not changed the original crystal structure of Maifan stone. Fig 6(B) shows diffraction peaks for quartz and potash feldspar, plagioclase, kaolin, type I cellulose and type II cellulose that appeared in the XRD spectra of AMD treated by Maifan stone loaded with SRB. Typical peaks characteristic of type I cellulose and type II cellulose appeared after AMD was treated with immobilized particles [44,45], indicating that the corncobs carbon source slowly released organic matter for the growth and metabolism of SRB. However, MnS and FeS peaks were observed after AMD treatment, indicating that SRB used corncobs as a carbon source to metabolize and reduce SO_4^{2-} to S^2, which reacted with heavy metal ions in AMD to form sulfide precipitates.

3.3.2 SEM analysis. The interior of Shandong Maifan stone and Maifan stone-sulfate-reducing bacterium-immobilized particles before and after AMD treatment and a scanning electron micrograph diagram of Maifan stone combined with SRB for the treatment of AMD are shown in Fig 7.

Fig 7(B) shows that the internal texture of Maifan stone-sulfate-reducing bacterium-immobilized particles is uniform and that pores developed, indicating that they had strong biological activity and basically met the requirements for AMD treatment. A comparison of Fig 7(B) and 7(c) shows that the internal structure of Maifan stone-sulfate-reducing bacterium-immobilized particles before and after the reaction underwent a great change. After the reaction part of the surface of the pore decreases in size and becomes uneven, the internal impurities increase, and the pores decrease. This finding shows that the removal of SO_4^{2-} by the Maifan stone-sulfate-reducing bacterium system occurs simultaneously on the surface and inside the particles. SO_4^{2-} enters the immobilized particles from the external water environment through the pores and forms S^{2-} by the sulfate-reducing bacterial dissimilatory reduction reaction. Fe^{2+} and Mn^{2+} in AMD combine with S^{2-} and produce sulfide precipitation in the particles, causing an increase in internal impurities. The pores decrease and even clogged. Many raised folds simultaneously formed. This phenomenon is caused by the toxic effect of Mn^{2+} adsorbed on the surface on SRB, which reduces the biological activity of SRB and produces a surface folding morphology [46]. In the Maifan stone-sulfate-reducing bacterium immobilized system, a series of physical, chemical and biological reactions occurred in the processing of AMD. Thus, the pollution of ions in the form of precipitation in the internal pores effectively inhibits the diffusion of pollutants. A comparison of Fig 7(a) and 7(d) reveals that after the dynamic test treatment of Maifan stone particles in AMD, which involves prolonged exposure to an acidic water environment their structure is eroded and destroyed and becomes looser, with a large amount of particle material on the surface. The results show that the sulfate-reducing bacterial dynamic column is not suitable for long-term reaction processes. A comprehensive comparison shows that Maifan stone sulfate-reducing bacterium-immobilized particles are more conducive to long-term resistance to AMD pollution load.

4. Conclusions

In this study, using the adsorption of Maifan stone and the reduction characteristics of SRB, based on immobilization technology, Maifan stone-sulfate-reducing bacterium-immobilized particles were employed to repair the pollution of Fe^{2+}, Mn^{2+}, and SO_4^{2-} in the acidic wastewater of coal mines. This approach can not only improve the activity of SRB to remove heavy metal cations and sulfate anions in AMD but also compensate for the lack of a single adsorption cation of Maifan stone. The synergistic effect of SRB and Maifan stones is more effective with a low cost. Based on the dynamic test and principles of dynamics and thermodynamics, the adsorption kinetics and adsorption thermodynamics equations of the treatment of AMD with Maifan stone and sulfate-reducing bacterium-immobilized particles were proposed for
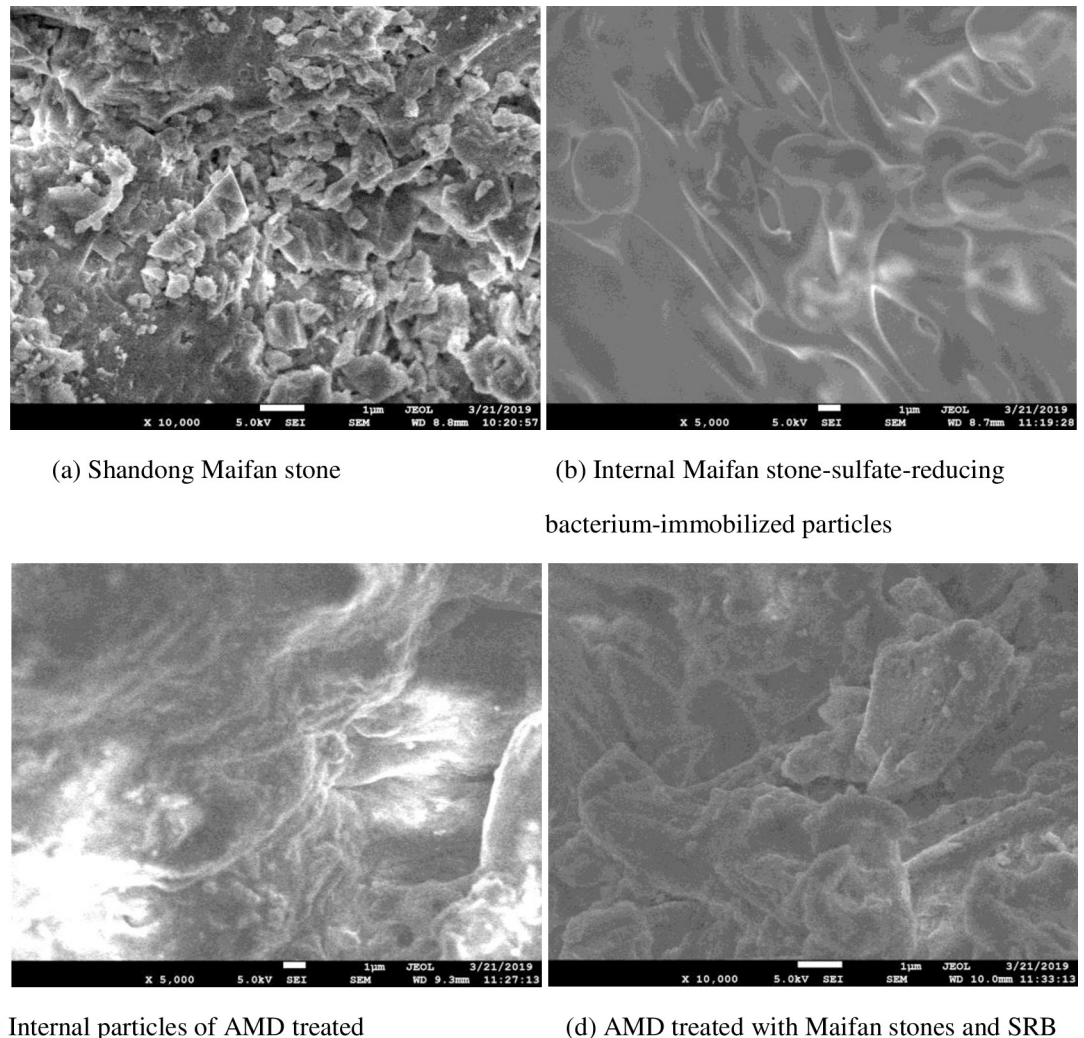
(a) Shandong Maifan stone   (b) Internal Maifan stone-sulfate-reducing

bacterium-immobilized particles

(c) Internal particles of AMD treated   (d) AMD treated with Maifan stones and SRB

Fig 7. SEM images of Maifan stones combined with SRB before and after AMD repair. (a) Shandong Maifan stone. (b) Internal Maifan stone-sulfate-reducing bacterium-immobilized particles. (c) Internal particles of AMD treated. (d) AMD treated with Maifan stones and SRB.

https://doi.org/10.1371/journal.pone.0261823.g007

the first time, revealing the mechanism of the efficient repair of AMD with Maifan stone and sulfate-reducing bacterium-immobilized particles. The following conclusions are presented:

1. By constructing Maifan stone-sulfate-reducing bacterium-immobilized particles in Dynamic Column 1 and Maifan stone-loaded SRB in Dynamic Column 2, the effects of Maifan stone-sulfate-reducing bacterium-immobilized particles and Maifan stone-loaded SRB on the remediation of Fe^{2+}, Mn^{2+} and SO_4^{2-} in AMD were compared. The Maifan stone-sulfate-reducing bacterium-immobilized particles in Dynamic Column 1 exhibited a better treatment effect, and the efficiencies for the removal of Fe^{2+}, Mn^{2+} and SO_4^{2-} were 90.51%, 85.75% and 93.61%, respectively. The pH of the wastewater was increased from 4.08 to 7.64.

2. The adsorption of Fe^{2+} and Mn^{2+} by Maifan stone-sulfate-reducing bacterium-immobilized particles conformed to the Langmuir adsorption isotherm model and first-order adsorption kinetics model. The Langmuir curve fitting equation for Fe^{2+} was $c_e/q_e = 6.43737c_e + 2.48397$

and $R^2 = 0.99754$. The Langmuir curve fitting equation for Mn^{2+} was $c_e/q_e = 4.8172c_e + 6.54707$, and $R^2 = 0.98428$. The equation for the first-order fit to the data for adsorption of Fe^{2+} was $q_t = 0.20428 \times (1-e^{-1.94074 \times 10^{-4}t})$, and $R^2 = 0.98428$. The equation for the first-order fit to the data for adsorption of Mn^{2+} was $q_t = 0.1924 \times (1-e^{-1.41278 \times 10^{-4}t})$, and $R^2 = 0.97054$.

3. The process of SO_4^{2-} reduction by SRB exhibited first-order reaction kinetics, and the fitting equation was $\ln c_t = 6.68937 - 3.19398 \times 10^{-4} t$, with $R^2 = 0.96865$, indicating that the electron acceptor was the main factor affecting the reduction of SO_4^{2-} by SRB.

Supporting information

S1 Data.
(XLSX)

Author Contributions

Data curation: Xuying Guo, Zhiyong Hu, Saiou Fu, Yanrong Dong, Guoliang Jiang, Ying Li.

Project administration: Xuying Guo.

Writing – original draft: Xuying Guo, Zhiyong Hu, Saiou Fu, Yanrong Dong, Guoliang Jiang, Ying Li.

Writing – review & editing: Xuying Guo.

References

1. Candeias C., et al. Acid mine drainage from the Panasqueira mine and its influence on Zêzere river (Central Portugal)[J]. Journal of African Earth Sciences, 2014, 99: p. 705–712.

2. Akcil A. and Koldas S., Acid Mine Drainage (AMD): causes, treatment and case studies[J].Journal of Cleaner Production, 2006. 14(12–13): p. 1139–1145.

3. Dutta M., et al., Acid mine drainage in an Indian high-sulfur coal mining area: Cytotoxicity assay and remediation study [J]. Journal of Hazardous Materials, 2020, 389: 121851. https://doi.org/10.1016/j.jhazmat.2019.121851 PMID: 31879117

4. Dhir B. Biotechnological tools for remediation of acid mine drainage (removal of metals from wastewater and leachate)[M]//Bio-Geotechnologies for Mine Site Rehabilitation. Elsevier, 2018: 67–82.

5. Mulopo J., et al. Recovery of calcium carbonate from steelmaking slag and utilization for acid mine drainage pre-treatment [J]. Water Science & Technology A Journal of the International Association on Water Pollution Research, 2012, 66(12):1296.

6. Tufaner F. Post-treatment of effluents from UASB reactor treating industrial wastewater sediment by constructed wetland[J]. Environmental technology, 2020, 41(7): p. 912–920. https://doi.org/10.1080/09593330.2018.1514073 PMID: 30122146

7. Klerk De, et al., The effect of rehabilitation measures on ecological infrastructure in response to acid mine drainage from coal mining [J]. Ecological Engineering, 2016, 95: p. 463–474.

8. Kkk A., et al. Evaluation of charcoal ash nanoparticles pollutant removal capacity from acid mine drainage rich in iron and sulfate[J]. Journal of Cleaner Production, 2020, 251: 119720.

9. Yang Yongjie, Simultaneous Adsorption Properties for Heavy Metal Ions by Mg-A1 Hydrotalcite, [D],2013.

10. Wulandari E, et al. Comparison of copper adsorption effectivity in acid mine drainage using natural zeolite and synthesized zeolite[C]//IOP Conference Series: Earth and Environmental Science. IOP Publishing, 2020, 473(1): 012143.

11. Zheng Q, et al. Experimental research on various slags as a potential adsorbent for the removal of sulfate from acid mine drainage[J]. Journal of Environmental Management, 2020, 270: 110880. https://doi.org/10.1016/j.jenvman.2020.110880 PMID: 32721319

12. Zhang Fan., et al. Advance of the treatment of heavy metal wastewater by adsorption [J].Chemical Industry and Engineering Progress,2013, 32(11): p. 2749–2756.

13. Pape P L, et al. Complete removal of arsenic and zinc from a heavily contaminated acid mine drainage via an indigenous SRB consortium[J]. Journal of Hazardous Materials, 2017, 321: p. 764–772. https://doi.org/10.1016/j.jhazmat.2016.09.060 PMID: 27720469

14. Ruehl MD., et al. Evaluation of organic carbon and microbial inoculum for bioremediation of acid mine drainage [J]. Minerals Engineering, 2020, 157:106554.

15. Liu Xiaoye, et al. High-efficiency treatment of low-sulfate in wastewater by a sort of SRB[C]//Proceedings of 2015 2nd International Workshop on Materials Engineering and Computer Sciences, 2015:35–39.

16. Jennyfer S., et al. Removal of Arsenic Using Acid/Metal-Tolerant Sulfate Reducing Bacteria: A New Approach for Bioremediation of High-Arsenic Acid Mine Waters[J].Water, 2017, 9(12):994.

17. Sarti A, et al. Anaerobic treatment of sulfate-rich wastewater in an anaerobic sequential batch reactor (AnSBR) using butanol as the carbon source[J]. Journal of Environmental Management, 2011, 92(6): p. 1537–1541. https://doi.org/10.1016/j.jenvman.2011.01.009 PMID: 21277676

18. Lang Xinghua. Study on Adsorption-Desorption of Plumbum and Cadmium by Immobilized Bacteria [D]. Northeastern University, 2007.

19. Liu Xing., et al. Optimization of the Parameters for Microalgae Immobilization and Analysis of Its Recovery Potential for Ammonia Nitroge in Wastewater[J].EnvironmentalScience,2019, 40(07): p. 3126–3134.

20. Hsu H F., et al. Simultaneous sulfate reduction and copper removal by a PVA-immobilized sulfate reducing bacterial culture[J]. Bioresource Technology, 2010, 101(12): p. 4354–4361. https://doi.org/10.1016/j.biortech.2010.01.094 PMID: 20153634

21. Sarti A, Zaiat M. Anaerobic treatment of sulfate-rich wastewater in an anaerobic sequential batch reactor (AnSBR) using butanol as the carbon source[J]. Journal of Environmental Management, 2011, 92(6): p. 1537–1541. https://doi.org/10.1016/j.jenvman.2011.01.009 PMID: 21277676

22. Wang Dong. Experiment on the Remediation Chlorobenzene-contaminated Groundwater by Using Immobilized Microorganisms [D]. JiLin University 2012.

23. Zhang M., et al. Preparation of metal-resistant immobilized sulfate reducing bacteria beads for acid mine drainage treatment[J]. Chemosphere, 2016, 154: p. 215–223. https://doi.org/10.1016/j.chemosphere.2016.03.103 PMID: 27058913

24. Wen Ke., et al. Physicochemical properties and adsorption performances of Nianzishan Maifan Stone in Qiqihar for heavy metal ions [J]. Acta Petrologica et Mineralogica,2016, 35(04): p. 712–720.

25. Zhao Zhe. Surface electrical property and adsorption performance of Maifan stone [J]. Journal of Natural Science of Heilongjiang University,2007, 4(03): p. 357–360.

26. Zhang Lehong., et al. Germination and Antioxidant Activity of Buckwheat Sprouts Cultivated in Maifanite Water [J]. Modern Food Science and Technology,2018, 34(07): p. 187–195+186.

27. Ma Puxi. Nitrate removal from groundwater using medical stone as carrier[D]. China University of Geosciences (Beijing),2013.

28. Jiang H, et al. Modification of polyurethane sponge filler using medical stones and application in a moving bed biofilm reactor for ex situ remediation of polluted rivers[J]. Journal of Water Process Engineering, 2021, 42: 102189.

29. C. F, et al. Bioremoval of arsenic and antimony from wastewater by a mixed culture of sulfate-reducing bacteria using lactate and ethanol as carbon sources[J]. International Biodeterioration & Biodegradation, 2018, 126: p.152–159.

30. Shi Yuchen, et al. Geological Characteristics and Physical-chemical Properties of Some Typical Maifan stone in Shandong[J].Shandong Land and Resources, 2000, p. 17–23.

31. Xia Changbin, Kinetic study on adsorption of Pb^{2+} on Maifan Stone[J].Environmental Chemistry., 2000 (05): p. 436–440.

32. Anandkumar B., et al., Corrosion behavior of SRB Desulfobulbus propionicus isolated from an Indian petroleum refinery on mild steel[J].Materials and Corrosion, 2012, 63(4): p. 355–362.

33. Kiran M.G., et al. Heavy metal removal from multicomponent system by sulfate reducing bacteria: Mechanism and cell surface characterization[J].Journal of Hazardous Materials, 2017, 324(Pt A): p. 62–70. https://doi.org/10.1016/j.jhazmat.2015.12.042 PMID: 26847522

34. Lin Hai, et al., Advances in Treatment of Acid Mine Drainage by Sulfate-Reducing Bacteria[J]. Environmental Protection Science, 2019, 45(05): p. 25–31.

35. Vossoughi M., et al. Performance of anaerobic baffled reactor treating synthetic wastewater influenced by decreasing COD/SO4 ratios[J].Chemical Engineering and Processing: Process Intensification, 2003, 42(10): p. 811–816.

36. Hallberg K.B, et al. Biological manganese removal from acid mine drainage in constructed wetlands and prototype bioreactors[J]. The Science of the total environment, 2005, 338(1–2): p. 115–124. https://doi.org/10.1016/j.scitotenv.2004.09.011 PMID: 15680632

37. Ai T, et al. A conceptual method to simultaneously inhibit methane and hydrogen sulfide production in sewers: The carbon metabolic pathway and microbial community shift[J]. Journal of environmental management, 2019, 246: p. 119–127. https://doi.org/10.1016/j.jenvman.2019.05.111 PMID: 31176177

38. Li Juan, et al., chemical properties of Maifan Stone and its application in water quality optimization[J]. Environmental Science & Technology, 2008, 10: p. 63–66+75.

39. Li X, et al. The bioenergetics mechanisms and applications of sulfate-reducing bacteria in remediation of pollutants in drainage: a review[J]. Ecotoxicology and environmental safety, 2018, 158: p. 162–170.

40. Feng Yun Gu. The Study on Nitrogen Source of Sulfate Reducing Bacteria Culture Medium and the Treatment Conditions of Acid Mine Drainage [D]. Jilin University,2017.

41. Di Junzhen., et al. Study on Treating Acid Mine Drainage by Strengthened Maifan Stone In-situ[J]. Non-metallic Minerals,2015, 38(02): p. 71–73.

42. Di Junzhen., et al. Treatment acid mine drainage by sulfate reducing bacteria using different biomass carbon sources[J]. Journal of China Coal Society,2019, 44(06): p. 1915–1922.

43. Wang Q, et al. Alginate/polyethylene glycol blend fibers and their properties for drug controlled release [J]. Journal of Biomedical Materials Research Part A, 2007, 82(1): p. 122–128. https://doi.org/10.1002/jbm.a.31075 PMID: 17269140

44. Neto W P F, et al. Extraction and characterization of cellulose nanocrystals from agro-industrial resi-due–Soy hulls[J]. Industrial Crops and Products, 2013, 42: p. 480–488.

45. Silvério HA, et al. Extraction and characterization of cellulose nanocrystals from corncob for application as reinforcing agent in nanocomposites[J]. Industrial Crops and Products, 2013, 44: p. 427–436.

46. Zhang Ye. Conversion of Hemicelluose into Furfural Using Inorganic Salt Catalysts [D]. An Hui University of Science and Technology,2014.